Biomacromolecules

Article

Cite This: Biomacromolecules XXXX, XXX, XXX−XXX

pubs.acs.org/Biomac

# Highly Stable, Coordinated Polymeric Nanoparticles Loading Copper(II) Diethyldithiocarbamate for Combinational Chemo/Chemodynamic Therapy of Cancer

Xinyu Peng,[†] Qingqing Pan,[†] Boya Zhang,[†] Shiyu Wan,[‡] Sai Li,[‡] Kui Luo,[§] Yuji Pu,*[,†] and Bin He[†]

[†]National Engineering Research Center for Biomaterials, Sichuan University, Chengdu 610064, China

[‡]School of Chemical Engineering, Sichuan University, Chengdu 610065, China

[§]Huaxi MR Research Center (HMRRC), Department of Radiology, West China Hospital, Sichuan University, Chengdu 610041, China

Supporting Information

**ABSTRACT:** Disulfiram (DSF) has excellent *in vitro* anticancer activity in the presence of Cu(II). The anticancer mechanism studies have demonstrated that copper(II) diethyldithiocarbamate, $Cu(DDC)_2$, is the crucial DSF's metabolite exhibiting anticancer activity. In this paper, highly stable polymeric nanoparticles were fabricated via a coordination strategy between Cu(II) and carboxylic groups in poly(ethylene glycol)-*b*-poly(ester-carbonate) (PEC) for efficient loading of $Cu(DDC)_2$, which was generated by the *in situ* reaction of DSF and Cu(II). The properties of nanoparticles such as drug loading contents, sizes, and morphologies could be tuned by varying the feeding ratios of DSF, Cu(II), and PEC. These Cu(II)/DDC-loaded nanoparticles showed excellent stability in both neutral and weak acidic solutions and under dilution. *In vitro* anticancer study established that Cu(II)/DDC-loaded nanoparticles could enable a combination therapy of $Cu(DDC)_2$-based chemotherapy and chemodynamic therapy mediated by bioavailable Cu(II) that was not in the form of $Cu(DDC)_2$. The *in vivo* antitumor results demonstrated that the Cu(II)/DDC-loaded nanoparticles showed superior antitumor efficacy to DSF/Cu(II). Our study provided a facile and effective strategy of highly stable coordination-mediated polymeric nanoparticles for combinational therapy of cancer.

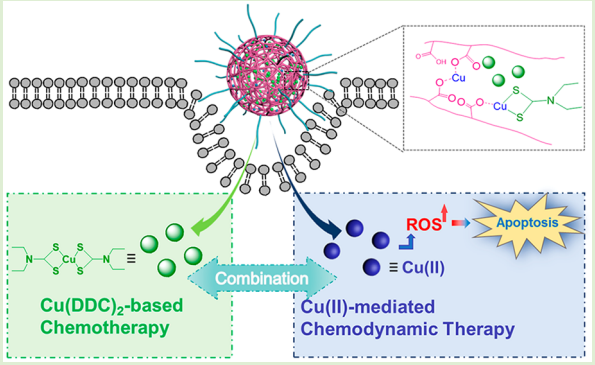


## 1. INTRODUCTION

Cancer is a global threat to human lives and drug resistance has been found during chemotherapy using clinical therapeutics. Since exploring new anticancer drugs encounters high costs and long testing periods, drug repurposing that screens the approved drugs for various diseases as candidate antineoplastic drugs is now a promising approach to address these issues.[1] Disulfiram (DSF) has been widely used as an antialcoholism drug for over 60 years. Recently, DSF is found to exhibit superb *in vitro* anticancer activity especially in the presence of Cu(II).[2,3] The anticancer mechanism of DSF is still being explored, and current study has established that DSF can target ALDH-positive cancer cells like cancer stem cells,[4,5] suppress proteasomes' activities to inhibit NF-$\kappa$B, PI3K, and TGF-$\beta$ pathways,[6,7] and induce the apoptosis of the tumor cells through a redox-related process.[8] The anticancer activity of DSF is Cu(II)-dependent.[9,10] A recent study has revealed that $Cu(DDC)_2$, the anticancer metabolite of DSF, could inhibit cancer by targeting the p-97-NPL4-UFDI protein complex, inducing accumulation of ubiquitinated proteins and a heat shock response.[11]

Despite the excellent *in vitro* anticancer activity, DSF still has some hurdles for its further *in vivo* cancer therapy. The main shortcoming of DSF is the rapid metabolism in blood,[12,13] and the enzymatic metabolites of DSF in liver are nontoxic to cancer cells.[14] To address the issue of extreme instability in blood, polymeric drug delivery systems (DDSs) have been developed to encapsulate DSF, alleviating the metabolite rate.[15−18] However, due to the intrinsic nonpolar structure and instability, the drug loading contents (DLCs) of DSF in these polymeric micelles were very low (usually 2−5%).[17,19,20]

Cu(II) is a vital factor for the high anticancer efficacy of DSF; however, in many previous research works, only DSF was loaded in DDSs and Cu(II) was neither loaded nor supplemented simultaneously. Although the copper concentration in many human tumor tissues is higher than that in normal tissues, the absolute Cu(II) concentration in tumor is still too low to inspire the therapeutic activity.[21] DDSs loading DSF alone without Cu(II) supplementation showed very

Received: March 14, 2019
Revised: May 15, 2019

Downloaded by UNIV AUTONOMA DE COAHUILA at 06:21:37:161 on May 30, 2019
from https://pubs.acs.org/doi/10.1021/acs.biomac.9b00367.


© XXXX American Chemical Society

DOI: 10.1021/acs.biomac.9b00367
Biomacromolecules XXXX, XXX, XXX−XXX

**Scheme 1. (A) Illustration of Cu(II)/DDC-Loaded Nanoparticle Preparation and the Proposed Interchain Coordination Effects for Efficient Loading of $Cu(DDC)_2$; (B) Anticancer Mechanism Illustration of Cu(II)/DDC-Loaded Nanoparticles**[a]

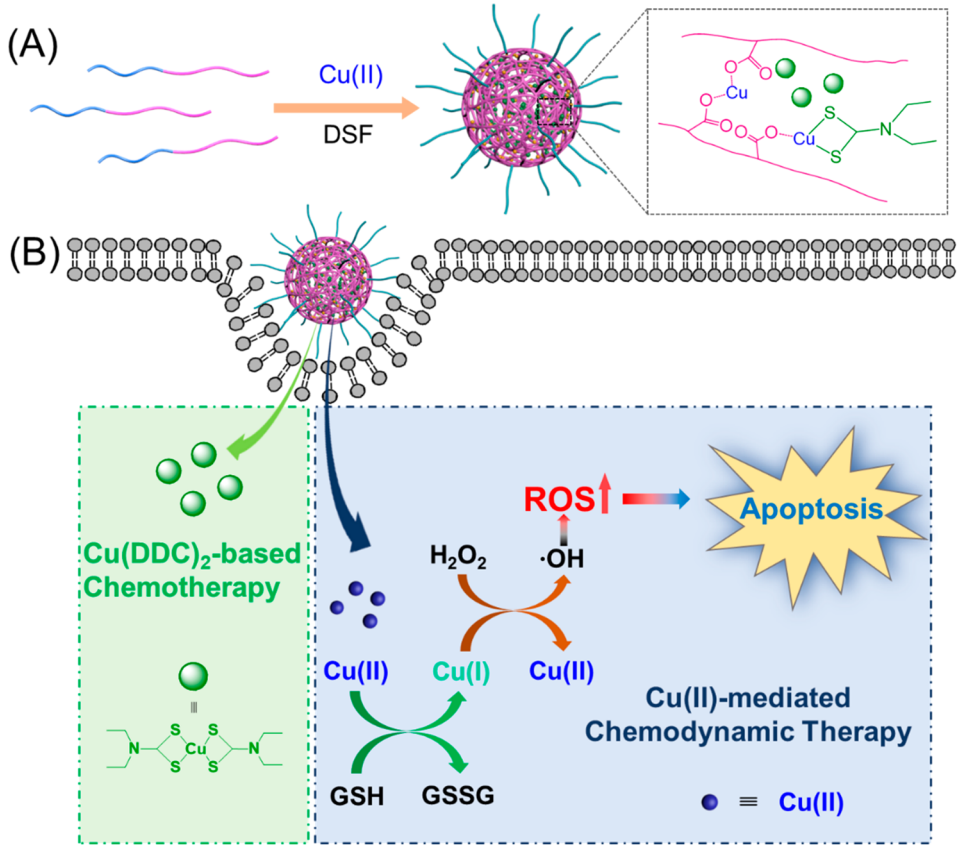


[a]After internalization into cancer cells, $Cu(DDC)_2$ was released to exert chemotherapy and Cu(II) that was available by GSH could induce ROS generation and apoptosis to fulfill chemodynamic therapy.

limited *in vivo* antitumor efficacy.[17,22] Therefore, exogenous Cu(II), such as copper gluconate, is orally taken to increase the copper concentration in tumor in clinical after DSF is intravenously administrated.[11] Although copper is an essential trace metal for human beings, uptake of large amounts of copper would lead to systemic toxicity. Besides, delivering DSF and Cu(II) simultaneously to tumor tissues with high concentrations via different ways is a challenge. Therefore, the strategy of delivering $Cu(DDC)_2$ instead of DSF had been developed recently.[23−25] Compared with the DSF-based DDSs, the delivery of $Cu(DDC)_2$ averted the inefficiency of DSF and additional supplementation of Cu(II).

The $Cu(DDC)_2$ complex was obtained by the reaction of Cu(II) and DSF (or sodium diethyldithiocarbamate, DDC). Chen et al. developed $Cu(DDC)_2$-loaded polymeric micelles loaded via the reaction of Cu(II) and DDC.[25] The micelles showed excellent inhibition to drug-resistant prostate cancer cells (DU145-TXR) in a manner of paraptosis. Although complexation of Cu(II) and oxygen atoms in poly(L-lactide) (PLA) or poly(ethylene glycol) (PEG) could stabilize $Cu(DDC)_2$, we postulated other stronger Cu(II) ligands containing polymer would not only codeliver Cu(II) and DSF but also enhance the stability of $Cu(DDC)_2$-loaded polymeric DDS.

In this study, we developed a highly stable coordinated nanoparticles to load $Cu(DDC)_2$ that was generated by the in situ reaction of Cu(II) and DSF. A carboxylic group containing amphiphilic copolymer, mPEG-*block*-poly(ester-carbonate) (PEC), was designed to form the stable nanoparticles by the coordination effects of Cu(II) and carboxylic groups in the polymer side chains, which could afford a core-cross-link-like architecture to enhance the stability of polymeric nanoparticles (Scheme 1A). The nanoparticles' properties and DLCs of $Cu(DDC)_2$ could be tuned by varying the feeding ratios of DSF, Cu(II), and PEC. These Cu(II)/DDC-loaded nanoparticles exhibited excellent stability in neutral and weak acidic conditions and against dilution. The anticancer mechanism study established that Cu(II)-mediated chemodynamic therapy[26−28] and $Cu(DDC)_2$-based chemotherapy were fulfilled in these Cu(II)/DDC-loaded nanoparticles (Scheme 1B). Benefiting from the excellent stability and combinational chemo/chemodynamic therapy, the Cu(II)/DDC-loaded nanoparticles showed superior *in vivo* antitumor effect to DSF/Cu(II).

## 2. EXPERIMENTAL SECTION

**2.1. Materials.** Methoxy poly(ethylene glycol) (mPEG, $M_n$ = 2000 Da) was purchased from Sigma-Aldrich Co. and used as received. All the other chemical reagents were from Tansoole Platform (Shanghai Titan Technology Co. Ltd.) and used as received. The solvents were obtained from Kelong Chemical Co. (Chengdu, China) and purified before use. Roswell Park Memorial Institute (RPMI) 1640 medium (HyClone), fetal bovine serum (FBS, HyClone), penicillin−streptomycin (HyClone), thiazolyl blue tetrazolium bromide (MTT, Energy Chemical), Annexin V-FITC/PI apoptosis detection kit (Dojindo Co.), PI/RNase staining buffer


DOI: 10.1021/acs.biomac.9b00367
Biomacromolecules XXXX, XXX, XXX−XXX

solution (BD Pharmingen), and reactive oxygen species (ROS) assay kit (Beyotime Biotechnology) were used for cell study.

**2.2. Characterization.** The chemical structures of the synthetic compounds and polymers were identified by $^1$H NMR (Bruker 400 MHz) and Fourier-transform infrared (FTIR) spectroscopy (Thermo Scientific Nicolet iS10). The molecular weights of polymers were characterized by gel permeation chromatography (GPC, Waters), and dimethylformamide (DMF) was used as the mobile phase. The sizes and $\zeta$-potentials of nanoparticles were measured by dynamic light scattering (DLS, Malven ZetasizerNano ZS). The size and morphology of nanoparticles were observed with transmission electron microscopy (TEM, JEOL JSM-6490LA, 100 kV, without negatively staining).

**2.3. Synthesis of Compound 1.** 2,2-Bis(hydroxymethyl)-propionic acid (50 g, 372 mmol) and potassium hydroxide (20.9 g, 373 mmol) were dissolved in DMF (200 mL). Benzyl bromide (76.51 g, 0.447 mmol) was added dropwise, and the mixture was stirred at 100 °C for 12 h. The solution was concentrated under vacuum after cooling and filtration. The residue was diluted with ethyl acetate (100 mL), washed with deionized water (3 × 100 mL) and brine, and dried with anhydrous $Na_2SO_4$. The product was obtained as a colorless crystal after recrystallization in toluene for three times (47.6 g, yield 57%).

**2.4. Synthesis of Compound 2.** To a solution of compound **1** (15.0 g, 66.0 mmol) and ethyl chloroformate (14.5 g, 133 mmol) in anhydrous THF (200 mL) was added trimethylamine (13.8 g, 136 mmol) dropwise in the solution in an ice bath. The solution was stirred at room temperature for 2 h. The white precipitate was filtered, and the solution was concentrated. The product was obtained as a colorless crystal after recrystallization in ethyl acetate for three times (12.7 g, yield 76%).

**2.5. Synthesis of PEC-Bn.** PEC-Bn was synthesized by a ring-opening polymerization using mPEG ($M_n$ 2000 Da) as a macro-initiator and stannous octoate ($Sn(Oct)_2$) as catalyst. mPEG (1.0 g, 0.5 mmol) was dried under vacuum at 100 °C for 4 h. Under argon atmosphere, L-lactide (0.866 g, 6.0 mmol), compound **2** (1.62 g, 6.5 mmol), and $Sn(Oct)_2$ (7.0 mg, 0.017 mmol) were added. Then the mixture was heated at 125 °C under vacuum for 24 h. The reaction was quenched by immersing the reaction tube into an ice bath. The crude product was dissolved in dichloromethane and precipitated in cold ethyl ether for three times. The product was dried under vacuum (3.45 g, yield 95%).

**2.6. Synthesis of PEC.** The mixture of PEC-Bn (3.0 g, 0.43 mmol) and Pd/C (0.3 g, 10%w/w) in dry DMF was stirred under $H_2$ atmosphere for 48 h. The hydrogen gas was freshly prepared by reaction of zinc and hydrochloric acid. Pd/C was filtered, and the solution was concentrated to obtain PEC (2.45 g, yield 98%).

**2.7. Preparation of Cu(II)/DDC-Loaded Nanoparticles.** A series of Cu(II) or Cu(II)/DDC-loaded nanoparticles were prepared by varying feeding ratios of COOH:DSF:Cu(II). Taking nanoparticle M2 as an example, the solution of PEC (10 mg, 20 $\mu$mol COOH), $CuCl_2$ (2.25 mg, 13.2 $\mu$mol), and DSF (1.95 mg, 6.6 $\mu$mol) in DMF (0.4 mL) was ultrasonicated for 2 h. The solution was then dropwise added into stirring ultrapure water (700 r/min). Afterward, the mixture was stirred for 12 h, dialyzed against ultrapure water for 24 h. The precipitate was removed by centrifugation and the supernatant was lyophilized to obtain M2. Cu(II)-loaded nanoparticles and other Cu(II)/DDC-loaded nanoparticles were prepared similarly.

**2.8. Drug Loading Contents and Drug Loading Efficiencies.** The drug loading contents (DLCs) and drug loading efficiencies (DLEs) of DDC in nanoparticles were measured by high-performance liquid chromatography (HPLC) with a reverse-phase C-18 column (Agilent) and a UV detector at 265 nm using mixed solvent of methanol and pH 7.0 PBS (80/20, V/V) as the mobile phase. The flow rate was 1.0 mL/min. The content of copper was measured by inductively coupled plasma atomic emission spectroscopy (ICP-AES). The DLCs and DLEs of Cu(II) or DDC were calculated by the following equations:

$$\text{DLCs (\%)} = \frac{\text{weight of DDC (or Cu) in NPs}}{\text{weight of NPs}} \times 100\%$$

$$\text{DLEs (\%)} = \frac{\text{weight of DDC (or Cu) in NPs}}{\text{weight of the feeding DSF (or Cu)}} \times 100\%$$

**2.9. Stability Study of Nanoparticles.** Cu(II) or Cu(II)/DDC-loaded nanoparticles were resuspended in different Acetate Buffered Saline (ABS buffers, pH 5.0, 6.8, and 7.4) at room temperature. At predetermined time intervals, the sizes and $\zeta$-potentials of nanoparticles were measured by DLS. Cu(II) or Cu(II)/DDC-loaded nanoparticles resuspended solutions (0.5 mg/mL) were diluted with PBS by 50 (0.01 mg/mL) and 500 times (0.001 mg/mL), and their sizes and $\zeta$-potentials at 0 and 24 h were measured at room temperature. The stability of the nanoparticles in the presence of proteins was studied in PBS (pH 7.4) with 10% FBS. The sizes of nanoparticles (0.5 mg/mL) were measured by DLS at 0 and 24 h.

**2.10. Drug Release.** The Cu(II)-loaded nanoparticles were dispersed in 1 mL of pH 7.4 PBS buffer with or without GSH (5 mM). Then the mixture was transferred into a dialysis bag (MWCO 1 kDa) and immersed in 25 mL of PBS (pH 7.4) with different GSH concentrations in the vials. The vials were placed in a shaking bed at 37 °C. At a predetermined time, 1 mL of the release media was taken out and fresh media was supplemented. The released Cu(II) content was measured by ICP-AES.

**2.11. Cell Culture.** The human nonsmall cell lung cancer cell line, A549, was cultured in RPMI 1640 medium with 10% FBS, 100 U/mL penicillin, and 100 U/mL streptomycin, and the solution was maintained at 37 °C in a humidified incubator with 5% $CO_2$.

**2.12. Cytotoxicity Test.** A549 cells were seeded in 96-well plates at a density of 4 × $10^3$ cells per well and cultured for 12 h. The cells were then cultured in the medium containing DSF, DSF/Cu(II), or Cu(II)/DDC-loaded nanoparticles at different DDC concentrations for 48 h. Cells were then treated with MTT containing serum-free medium (0.5 mg/mL, 100 $\mu$L) for 4 h. The purple formazan crystals were dissolved in dimethyl sulfoxide (DMSO, 150 $\mu$L) and the absorbance at 490 nm was measured on a microplate reader (Thermo Scientific MK3). The cytotoxicities of the polymer PEC and Cu(II)-loaded nanoparticles were tested similarly.

**2.13. Cellular Uptake of RhB-Loaded Nanoparticles.** Rhodamine B-loaded PEC nanoparticles were prepared according to our previous study.[29] The cellular uptake of the nanoparticles was studied by confocal laser scanning microscopy (CLSM).

**2.14. Intracellular Copper Content Test.** A549 cells were seeded in 6-well plates (5 × $10^5$ cells per well) and cultured for 12 h. Afterward, cells were treated with medium containing $CuCl_2$, Cu(II)/DSF, Cu(II)-loaded nanoparticles, or different Cu(II)/DDC-loaded nanoparticles (Cu(II) concentration: 2 $\mu$g/mL) for 4 h. Cells were harvested and counted, washed twice by PBS, and digested by the digestion solution containing 65% nitric acid and 15% $H_2O_2$ overnight at 65 °C. The lysate was diluted to a final volume of 10 mL, and Cu content was measured by ICP-AES. The Cu(II) levels in cells were expressed as Cu content (ng) per $10^4$ cells.

**2.15. Apoptosis Study.** A549 cells were seeded in 6-well plates (2 mL per well, 2.5 × $10^5$ cells) and cultured for 12 h. The culture medium was removed, and the cells were treated with medium containing DSF, different Cu(II)/DDC loaded nanoparticles, or Cu(II)/DSF (DSF concentration: 20 ng/mL) for 48 h. Cells were harvested and washed twice by PBS. For the apoptosis study, cells were then suspended in a binding buffer provided by the Annexin V-FITC/PI apoptosis detection kit as the manufacture's protocols. The cells were then mixed with Annexin V-FITC and PI, incubated in the dark at RT for 15 min, and analyzed by a BD Accuri C6 flow cytometer.

**2.16. Intracellular ROS Detection by DCFH-DA.** A549 cells were seeded in glass bottom dishes (1 mL per dish, 1 × $10^5$ cells) and cultured for 24 h. The cells were then treated with a medium containing Cu(II)/DDC-loaded nanoparticles, DSF/Cu(II) (DSF concentration: 10 ng/mL), Cu(II)-loaded nanoparticles, or $CuCl_2$ (Cu(II) concentration: 3 $\mu$g/mL) for different times. Thereafter, cells



DOI: 10.1021/acs.biomac.9b00367
Biomacromolecules XXXX, XXX, XXX−XXX

were incubated with DCFA-DA (10 $\mu$M) for 20 min and washed with PBS for three times. The intracellular ROS signal was observed by CLSM.

**2.17. *In Vivo* Antitumor Efficacy.** All animal experiments were performed in accordance with the Guidelines for Care and Use of Laboratory Animals of West China Hospital, Sichuan University and approved by the Animal Ethics Committee of China.[30] Female Balb/C nude mice (4−5 weeks of age, 18−22 g) were purchased from Chengdu Dashuo Experiment Animal Co. Ltd. $1.0 \times 10^6$ A549 cells were inoculated at the right flank of mice to build the A549 tumor model. After tumor growth reached about 100 $mm^3$, the mice were randomly divided into 3 groups ($n$ = 6) and treated with saline (by intravenous injection, i.v.), DSF/Cu(II) (DSF, 10 mg/kg, i.v.; copper gluconate, 1.5 mg/kg, oral administration), and M3 (1 mg/kg in DSF dosage, i.v.) on days 0, 4, 8, 12. The body weights and tumor volumes of tumor-bearing mice were recorded every 4 days. The tumor volumes and tumor inhibition rates were calculated according to our previous study.[31] The H&E staining study of tumor and normal organs was carried out according to our previous literature.[32]

**2.18. Statistical Analysis.** All mean values ± SD reported in results section were compared by Student's $t$ test. $P$ values of no more than 0.05 were considered significant differences.

## 3. RESULTS AND DISCUSSION

**3.1. Polymer Synthesis and Design.** The biodegradable polymer mPEG-*b*-poly(ester-carbonate), PEC, was synthesized as shown in Scheme 2. Polyesters and polycarbonates are employed because they are biodegradable and biocompatible polymers and extensively studied in various biomedical applications.[33−35] In addition, PLA was used to endow hydrophobicity to efficiently load hydrophobic $Cu(DDC)_2$; polycarbonate was designed to load Cu(II) mainly by coordination interactions between carboxylic groups in polycarbonate and Cu(II). A cyclic carbonate monomer, compound **2** in Scheme 2A, was first synthesized by the cyclization of compound **1**, which was obtained by a benzyl protection reaction of 2,2-bis(hydroxymethyl)propionic acid. Compound **2** and L-lactide (LA) were then copolymerized by ring-opening polymerization using mPEG ($M_n$ 2000 Da) as a macroinitiator and $Sn(Oct)_2$ as a catalyst to give PEC-Bn. The benzyl groups in PEC-Bn were deprotected by Pd/C to give PEC that contains free carboxylic groups.

**Scheme 2. Synthesis of Monomer (A) and PEG-*b*-poly(ester-carbonate) PEC (B)**

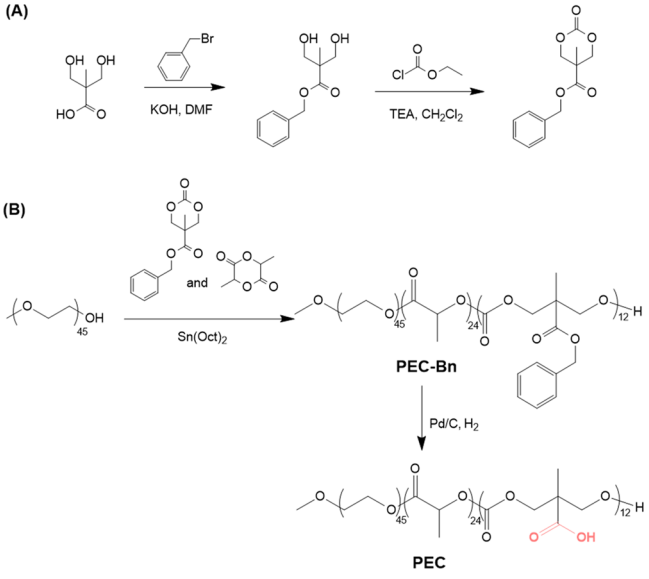


The structures of the carbonate monomer and copolymers were characterized by $^1$H NMR and FTIR (Figures 1 and S1−S2). The monomer composition in PEC was calculated by NMR; the degrees of polymerization of **2** and LA were 11 and 22, respectively (Table S1). The molecular weight of PEC-Bn was determined by GPC (Figure S3 and Table S1) and the molecular weight was ∼5 kDa. The successful deprotection of PEC-Bn was verified by NMR. As shown in Figure 1, the peaks that are corresponding to the benzyl groups at 7.33 ppm disappeared in the NMR spectrum of PEC, which was consistent with the results in the previous literature.[36,37]

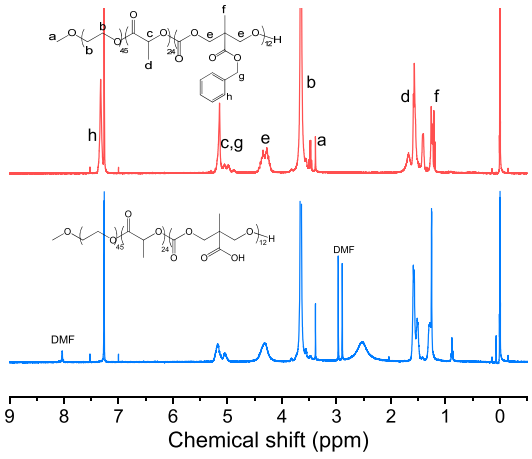


**Figure 1.** $^1$H NMR spectra of PEC-Bn and PEC in $CDCl_3$.

**3.2. Stability of Coordination-Mediated Cu(II)-Loaded Polymeric Nanoparticles.** We first studied the Cu(II) loading efficiency of carboxyl-containing PEC by coordination effects. We found that PEC alone could not self-assemble into nanoparticles (data not shown here), which were probably due to the negative charge repulsion of carboxylic groups and poor hydrophobicity of PEC. However, nanoparticles were formed after the addition of Cu(II), which was verified by the detection of nanoparticles by DLS. The driving force of nanoparticle formation was mainly attributed to the intermolecular coordination effects of carboxylic groups and Cu(II) (Figure 2A).[38] Although the complexation of Cu(II) and oxygen atoms in PEC could facilitate Cu(II) loading,[25] we would attribute the nanoparticle formation mainly to the coordination effects owing to the excellent nanoparticle under dilution, which will be discussed later.

A series of Cu(II)-loaded polymeric nanoparticles were prepared by varying the feeding molar ratios of carboxylic groups (COOHs) in PEC to Cu(II) to study the Cu(II) loading efficiency. The successful loading of Cu(II) was confirmed and quantitively determined by ICP-AES, and the Cu(II) concentrations in these nanoparticles were in the range 0.19−0.23 mM (Table S2). The copper content showed an increase trend with increasing feeding ratio of Cu(II) to COOH when the ratio was less than 1:1 (drug loading contents (DLCs) ranges from 2.66% to 3.10%, Figure 2B). When the feeding ratio of Cu(II)/COOH was 1:1, the Cu(II) concentration was the highest (DLC of 3.10%, 0.23 mM) in the Cu(II)-loaded polymeric nanoparticles. However, a further increase of Cu(II)/COOH ratio lead to a decrease of DLC of Cu(II) (2.68%). The trend of drug loading efficiencies (DLEs)


DOI: 10.1021/acs.biomac.9b00367
Biomacromolecules XXXX, XXX, XXX−XXX

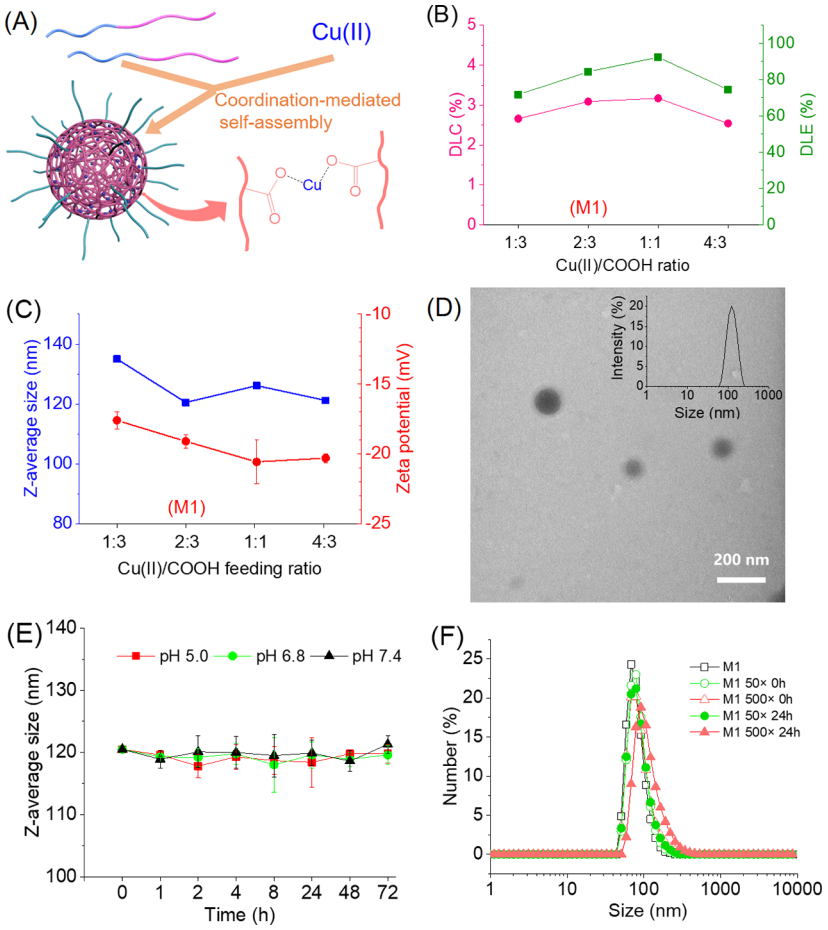


**Figure 2.** Preparation and characterization of the Cu(II)-loaded polymeric nanoparticles. (A) The illustration of the Cu(II)-loaded nanoparticle preparation by coordination effects. The impact of Cu(II)/COOH feeding molar ratios on DLCs and DLEs (B), and the sizes and ζ-potentials (C) of Cu(II)-loaded nanoparticles. (D) TEM image of nanoparticles M1 (the Cu(II)/COOH feeding molar ratio was 2:3); the inset shows the size results by DLS. (E) The changes of *Z*-average sizes of M1 over time in different pH conditions. (F) The size changes of M1 after dilution for 50 and 500 times at 0 and 24 h.

was similar to that of DLCs in the Cu(II)-loaded nanoparticles, and the DLEs were in the range 17.9%−71.8%. The effect of Cu(II)/COOH ratios on the sizes and ζ-potentials of Cu(II)-loaded nanoparticles was also studied (Figure 2C). We found that the feeding Cu(II)/COOH ratios had a subtle effect on the nanoparticles' sizes and ζ-potentials. The nanoparticles showed average *Z*-average sizes of 120−135 nm, and ζ-potentials were in the range −17.6 to −20.5 mV.

The typical TEM image of Cu(II)-loaded nanoparticle M1 (Cu(II)/COOH = 2:3) is shown in Figure 2D. Obviously, M1 showed a core−shell structure with a size less than 200 nm, which was consistent with the DLS result (the inset in Figure 2D). The core in the TEM image was ascribed to Cu(II) and poly(ester-carbonate) blocks of PEC, and the shell was a hydrophilic PEG layer.

The stability of the Cu(II)-loaded nanoparticles was first investigated by studying the changes of nanoparticles' sizes and ζ-potentials at predetermined time intervals in different pH conditions (Figure 2E and Figure S8A). The sizes and ζ-potentials of M1 showed negligible changes over 72 h in all pH conditions (pH 7.4, 6.8, and 5.0), indicating the high stability of Cu(II)-coordinated polymeric nanoparticles. We then studied the stability of Cu(II)-loaded nanoparticles against dilution.[39] As shown in Figure 2F, the sizes showed weak variations at 0 and 24 h after 50- or 500-times dilution (the initial concentration of M1 was 0.5 mg/mL). Together, these results established that Cu(II)-coordinated polymeric nanoparticles exhibited excellent stability.

**3.3. Drug Loading Properties of Coordination-Mediated Cu(II)/DDC-Coloaded Polymeric Nanoparticles.** Inspired by the excellent stability of Cu(II)-coordinated PEC nanoparticles and the intrinsic anticancer effect of $Cu(DDC)_2$, we then evaluated the capacity of PEC to coload Cu(II) and DSF. Because the reaction between DSF and Cu(II) was very rapid (within several minutes, Figures S4 and S5), $Cu(DDC)_2$ could be generated and loaded *in situ* during the nanoparticle formation, which was mainly driven by the coordination effects between COOH and Cu(II) as well as hydrophobic interactions between PEC and $Cu(DDC)_2$ (Scheme 1A). The obtained nanoparticles were denoted as Cu(II)/DDC-loaded nanoparticles. The as-prepared typical nanoparticles' suspensions are shown in Figure S6, and precipitation of $Cu(DDC)_2$ was not observed. The colors of the nanoparticle suspensions were more brown and darker with increased DSF/Cu(II) feeding molar ratios, suggesting a higher loading content of $Cu(DDC)_2$.

A series of Cu(II)/DDC-loaded nanoparticles were fabricated by varying the feeding ratios of DSF/Cu(II)/COOH (Table S2). The drug loading contents (DLCs) and the drug loading efficiencies (DLEs) of DDC, $Cu(DDC)_2$, and


DOI: 10.1021/acs.biomac.9b00367
*Biomacromolecules* XXXX, XXX, XXX−XXX

Cu(II) in the Cu(II)/DDC-loaded nanoparticles are summarized in Table S2 and Figure 3. When the Cu(II)/COOH ratio

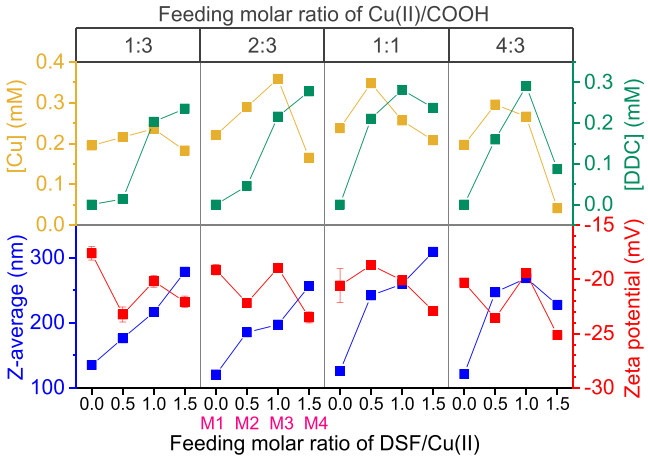


**Figure 3.** Impact of feeding molar ratios of DSF/Cu(II)/COOH on the nanoparticle properties (*Z*-average sizes, ζ-potentials, Cu(II) and DDC concentrations) of Cu(II)/DDC-loaded nanoparticles. Generally, when the feeding molar ratio of Cu(II)/COOH was fixed, higher Cu(II) and DDC loading contents could be obtained when DSF/Cu(II) was 1:1. (M1−M4 represent the nanoparticles prepared by fixed feeding Cu(II)/COOH molar ratio of 2:3 and different feeding amounts of DSF).

was fixed, the DLCs of Cu(II) and DDC would first increase and then decrease with the increasing DSF/Cu(II) ratios from 0:1 to 3:2 (0 to 1.5 in Figure 3). The low DLCs of Cu(II) and DDC in the high DSF/Cu(II) ratio of 1.5 (Cu(II)/COOH was 1:1 or 4:3) were ascribed to that excessive DSF resulted in precipitation of $Cu(DDC)_2$ during nanoparticle preparation. The highest DLCs of Cu(II) and $Cu(DDC)_2$ in these nanoparticles were about 4.55% and 10.0%, respectively.

The effect of the feeding molar ratios on the sizes and ζ-potentials of Cu(II)/DDC-loaded nanoparticles was also studied. As shown in Figure 3, the *Z*-average sizes of nanoparticles increased with the increasing DSF/Cu(II) ratios from about 100 to 300 nm, except that the nanoparticles prepared with a feeding DSF/Cu(II)/COOH ratio of 3:2:1.5, which showed smaller size because of its extremely low DLCs of Cu(II) and DDC that was induced by large amount of precipitation of $Cu(DDC)_2$. The ζ-potentials of Cu(II)/DDC-loaded nanoparticles showed no obvious change patterns and they were in the range from −18 to −25 mV. We then chose Cu(II)/DDC-loaded nanoparticles (M2−M4) that were prepared with a feeding Cu(II)/COOH ratio of 2:3 for further study due to the highest $Cu(DDC)_2$ loading content in M4 and the obvious differences of $Cu(DDC)_2$ loading contents in three nanoparticles.

Figures 4A1, B1, and C1 show the TEM images of Cu(II)/DDC-loaded nanoparticles M2, M3, and M4, respectively. Obviously, Cu(II)/DDC-loaded nanoparticles (M2−M4) were distinct from the corresponding Cu(II)-loaded nanoparticle M1 in size and morphology (Figure 2D). The nanoparticles sizes by TEM increased with increasing feeding ratio of DSF/Cu(II), which was consistent with the DLS results (Figure 3). Nanoparticles M2−M4 showed different morphologies due to the different Cu(II) and $Cu(DDC)_2$ loading contents. The morphologies of Cu(II)/DDC-loaded nanoparticles changed from spherical to irregular with increasing DSF/Cu(II) ratios. The successful loading of

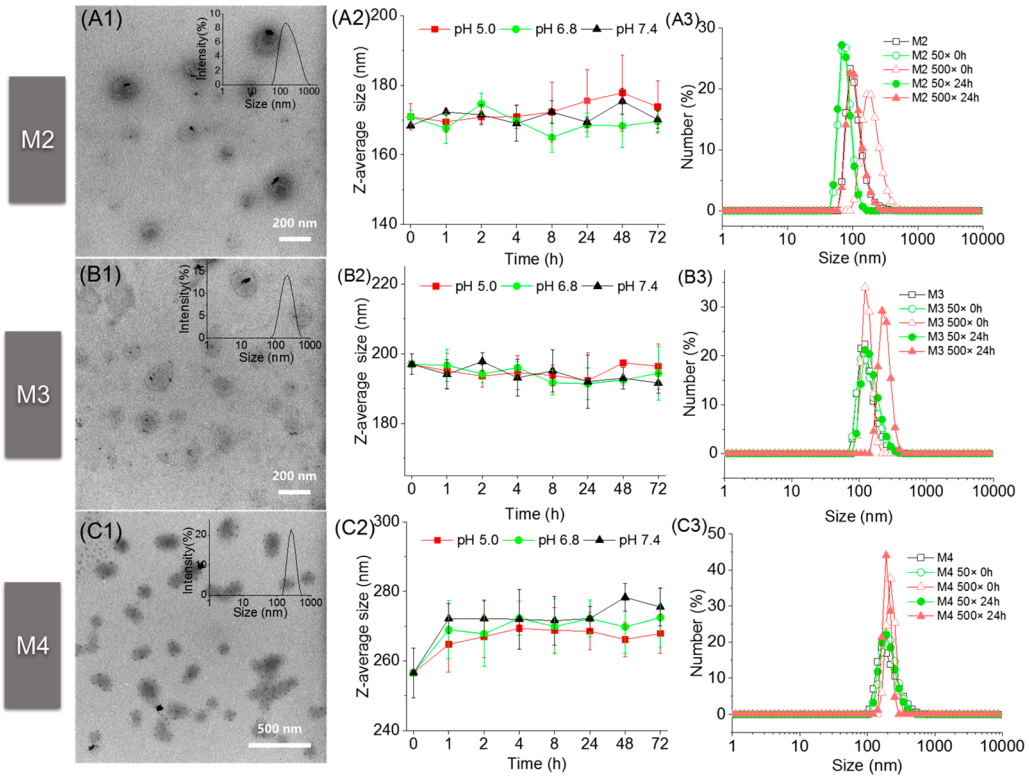


**Figure 4.** TEM images of nanoparticles M2 (A1), M3 (B1), and M4 (C1); the insets are the corresponding DLS results. Size changes of M2−M4 in different pH conditions (A2, B2, and C2) and under dilution (A3, B3, and C3).



DOI: 10.1021/acs.biomac.9b00367
*Biomacromolecules* XXXX, XXX, XXX−XXX

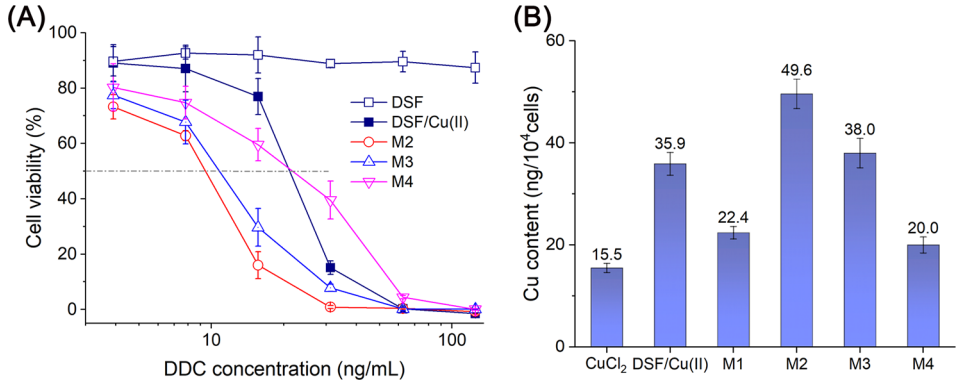


**Figure 5.** (A) Cell viabilities of A549 cells treated with DSF, DSF/Cu(II) (DSF and Cu(II) in equimolar amount), and Cu(II)/DDC-loaded nanoparticles M2−M4 for 48 h. (B) Intracellular Cu contents of A549 cells treated with different formulations at a Cu(II) concentration of 2 $\mu$g/mL for 4 h ($n$ = 3).

Cu(II) and $Cu(DDC)_2$ were further confirmed by scanning transmission electron microscopy (Figure S7).

Nanoparticle stability plays an important role in further long blood circulation, which is the key to its *in vivo* antitumor efficiency. Inspired by the excellent stability of the aforementioned coordination-mediated Cu(II)-loaded polymeric nanoparticles, we studied the stability of these Cu(II)/DDC-loaded nanoparticles in different pH conditions. Nanoparticles M2−M4 were treated with PBS at different pH (pH 7.4, 6.8, and 5.0) and their sizes and $\zeta$-potentials were measured at different time points (Figures 4A2, B2, C2, and Figure S8B−D). Notably, all nanoparticles showed excellent stability in all pH conditions over 72 h, except that M4 showed a slight increase in size at 1 h and M2−M4 showed slight increases in $\zeta$-potential at 1−4 h. Despite a slight disturbance in sizes and $\zeta$-potentials in the initial stage, the nanoparticles were stable in sizes and $\zeta$-potentials over 72 h. The dilution study also established that Cu(II)/DDC-loaded nanoparticles were stable after even 50- to 500-times dilution after 24 h (the initial nanoparticles concentrations were 0.5 mg/mL, Figures 4A3, B3, and C3).

The stability of Cu(II)/DDC-loaded nanoparticles under 10% FBS condition was also carried out (Figure S9). After a 24 h incubation, M3 and M4 showed slight size increase and were still monodisperse, suggesting excellent stability in the presence of 10% FBS. In contrast, M1 and M2 showed poorer stability in the condition of 10% FBS and the sizes were polydisperse at 24 h. The poorer stability of M1 and M2 in FBS conditions were probably ascribed to the Cu(II)-mediated interaction with FBS. In M3 and M4, however, hydrophobic interactions between $Cu(DDC)_2$ and polymers may stabilize the nanoparticle and hinder the Cu(II)-FBS interactions. Collectively, these results suggested that Cu(II)/DDC-loaded nanoparticles were stable in neutral, weak acidic environments and under dilution. M3 and M4 showed excellent stability even in the presence of serum.

Given the excellent stability of Cu(II)/DDC-loaded nanoparticles, we assumed that their *in vitro* drug release behaviors in different pH conditions may be very slow. The especially low concentration of DDC is hard to be detected by HPLC, therefore, the drug release of DDC was not shown here. Since Cu(II) is an oxidant and GSH acts reducing agents to balance the redox homeostasis and has much higher concentration in cancer cells, we then studied whether GSH could affect the release of Cu(II). Notably, the Cu(II)-loaded nanoparticles showed different release behavior in the presence and absence of 10 mM GSH (Figure S10). In the presence of GSH, a burst release of Cu(II) was observed after 8 h, suggesting the GSH-sensitiveness of the Cu(II)-coordinated polymeric nanoparticles.

**3.4. *In Vitro* Anticancer Efficacy of Cu(II)/DDC-Loaded Nanoparticles.** Before the *in vitro* anticancer study of Cu(II)/DDC-loaded PEC nanoparticles, the cytotoxicity of PEC against normal cells was studied by an MTT assay to evaluate its cytocompatibility. NIH 3T3 cells were treated with cell culture medium with varying concentrations of PEC for 48 h. As shown in Figure S11, the viability of NIH 3T3 cells was PEC dose-dependent; 85.0% and 70.7% cells were alive after the treatment with PEC at polymer concentrations of 100 and 250 $\mu$g/mL, respectively. The cytotoxicity results suggested that PEC showed good cytocompatibility.

The *in vitro* anticancer activity of DSF, DSF/Cu(II), and Cu(II)/DDC-loaded nanoparticles M2−M4 in A549 cells was then evaluated by an MTT assay. As shown in Figure 5A, DSF alone showed poor anticancer activity due to the shortage of extracellular Cu(II). However, DSF/Cu(II) showed significantly enhanced anticancer activity (IC50:21.0 ng/mL) due to the presence of the same molar amount of extracellular Cu(II), consistent with many previous reports that DSF showed superb *in vitro* anticancer efficacy in the presence of sufficient Cu(II). M4 showed comparable anticancer activity to DSF/Cu(II) with an IC50 value of 21.7 ng/mL. Interestingly, M2 and M3 with less DLC of $Cu(DDC)_2$ than M4 showed lower IC50 values of 9.4 and 10.7 ng/mL, respectively, about half of the IC50 value of DSF/Cu(II), suggesting better anticancer activity than DSF/Cu(II). The best anticancer activity of M2 was aberrant to its lowest DLC of $Cu(DDC)_2$. Therefore, we envisaged that high DLC of Cu(II) could fulfill chemodynamic therapy since the cytotoxicity of PEC was low.

Cu(II) is an essential element of life; however, deficient or excessive copper could lead to corresponding diseases. Elevated copper contents have been found in various human tumor tissues relative to normal tissues. The high copper concentration in tumor tissue is essential to Cu(II)-involved enzymatic activity and angiogenesis.[21] In addition, excessive Cu(II) that acts as oxidant could lead to oxidative stress in cells.[40] For example, Ma et al. had recently reported that Cu(II)-amino acid nanoparticles could efficiently inhibit cancer cells by Cu(II)-mediated chemodynamic therapy where Cu(II) reacted with intracellular GSH and $H_2O_2$


DOI: 10.1021/acs.biomac.9b00367
Biomacromolecules XXXX, XXX, XXX−XXX

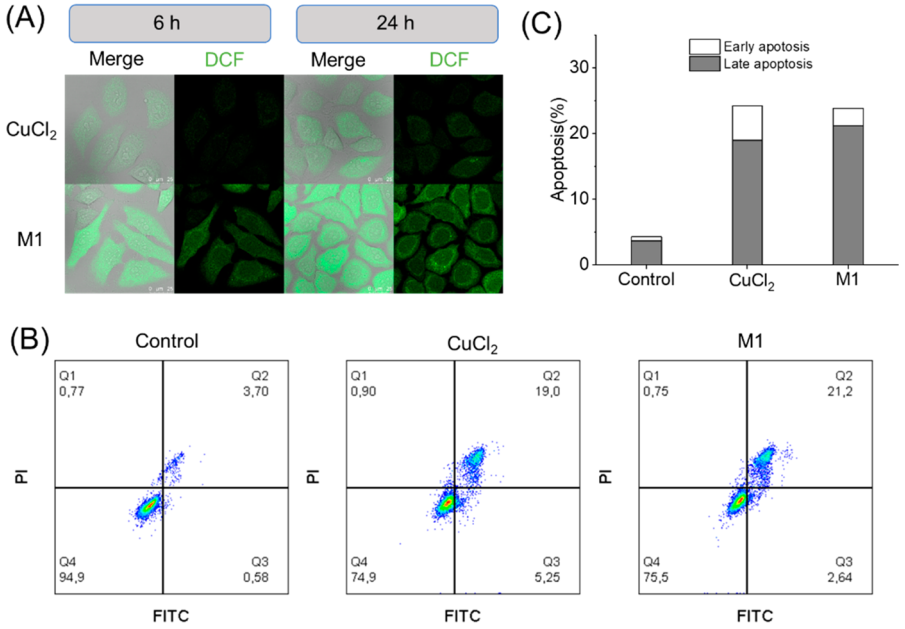


**Figure 6.** (A) CLSM images of A549 cells treated with $CuCl_2$ and M1 at the same concentrations for 6 and 24 h. (B, C) Apoptosis rates of A549 cells treated with $CuCl_2$ and M1 at a Cu(II) concentration of 3 $\mu$g/mL for 48 h.

successively to lead to upregulation of ROS that induces cancer cell apoptosis (Scheme 1B).[41]

The cellular uptake behaviors of the coordination-mediated nanoparticles were first studied by CLSM. Because of the very low fluorescence of Cu(II)/DDC-loaded nanoparticles, Rhodamine B-loaded PEC nanoparticles was prepared for CLSM study. Like other polymeric nanoparticles internalized by endocytosis, the Rhodamine B-loaded nanoparticles showed a time-dependent internalization (Figure S12), demonstrating the efficient cellular uptake of the polymeric nanoparticles. Second, the intracellular copper contents of A549 cells treated with M2−M4 as well as DSF and DSF/Cu(II) were studied; the results are shown in Figure 5B. DSF/Cu(II) showed significantly enhanced Cu(II) uptake relative to $CuCl_2$, suggesting that DSF facilitated the cellular uptake of Cu(II).[42] M2 showed the highest Cu(II) uptake due to its high Cu(II) loading content, and the intracellular copper contents of these groups were in the order of M2 > M3 ≈ DSF/Cu(II) > M1 ≈ M4 > $CuCl_2$. The high intracellular copper contents induced by M2 and M3 were consistent with their excellent *in vitro* anticancer activity, confirming our envisagement that high DLC of Cu(II) could inhibit cancer cells.

**3.5. Cu(II)-Loaded Nanoparticles Induce Intracellular ROS Generation and Cancer Cell Apoptosis.** To demonstrate the chemodynamic therapy induced by Cu(II) uptake, we first studied the cytotoxicity of Cu(II)-loaded nanoparticles M1 as well as $CuCl_2$ against A549 cells. As shown in Figure S13, $CuCl_2$ showed a dose-dependent toxicity to A549 cells, indicating the toxicity of high concentration of Cu(II). M1 showed significantly enhanced cancer cell inhibition relative to $CuCl_2$, suggesting the PEC-enhanced Cu(II)-mediated toxicity. The intracellular Cu content study demonstrated that M1 showed elevated cellular uptake of Cu(II) to that of $CuCl_2$ (Figure 5B), implying the enhanced nanoparticle-mediated cellular uptake of Cu(II). Considering the low cytotoxicity of PEC, the enhanced cytotoxicity of M1 was mainly ascribed to the higher Cu(II) uptake of M1.

Cu(II)-mediated chemodynamic therapy exerted anticancer activity by generating highly cytotoxic ROS like ·OH that could destroy proteins, lipids, and DNA, inducing cell apoptosis (Scheme 1B).[41,43,44] The intracellular ROS generation could be detected by a probe 2′,7′-dichlorodihydrofluorescein diacetate (DCFH-DA), a small molecule that could be taken by cells and the followed oxidation by intracellular ROS could give 2′,7′-dichlorofluorescein (DCF) with green fluorescence.[45,46] Cells treated with M1 showed stronger fluorescence intensity than those treated with $CuCl_2$ at 6 and 24 h (Figure 6A), demonstrating the more ROS generation induced by higher cellular uptake of Cu(II). An FITC-PI assay was carried out to assess the M1-induced apoptosis. As shown in Figure 6B,C, M1 and $CuCl_2$ induced comparable cell apoptosis (23.8% vs 24.2%) at the same Cu(II) concentration. However, cells treated with M1 were more in the stage of late apoptosis (21.2% vs 19.0%), confirming its higher cytotoxicity.

**3.6. Cu(II)/DDC-Loaded Nanoparticles Inhibit Cancer Cells via a Chemo/Chemodynamic Combinational Therapy.** We studied the anticancer mechanism of Cu(II)/DDC-loaded nanoparticles by investigating the ROS generation induced by DSF/Cu(II) and Cu(II)/DDC-loaded nanoparticles. The CLSM results showed that M2 treated cells had the strongest green fluorescence at 6 and 24 h (Figure 7A), demonstrating that the most ROS was generated. Similar results were obtained in the flow cytometry (Figure S14).

The apoptosis study showed that the apoptosis rates of DSF, DSF/Cu(II), M2, M3, and M4 were 12.2%, 16.9%, 17.6%, 13.2%, and 4.9%, respectively (Figure 7B). Notably, M4, which had the highest DLC of DDC and thereby very low DLC of Cu(II) that are not in the form of $Cu(DDC)_2$ because DDC was a strong chelator of Cu(II), induced very low and comparable apoptosis rate relative to control group (3.7%), indicating that $Cu(DDC)_2$ per se cannot generate intracellular ROS, which was consistent with the previous report by Wang et al.[14] Since DDC was a strong chelator of Cu(II), $Cu(DDC)_2$ could not react with GSH. Therefore, $Cu(DDC)_2$ alone could not induce ROS generation in cells, and M4 with the highest


DOI: 10.1021/acs.biomac.9b00367
Biomacromolecules XXXX, XXX, XXX−XXX

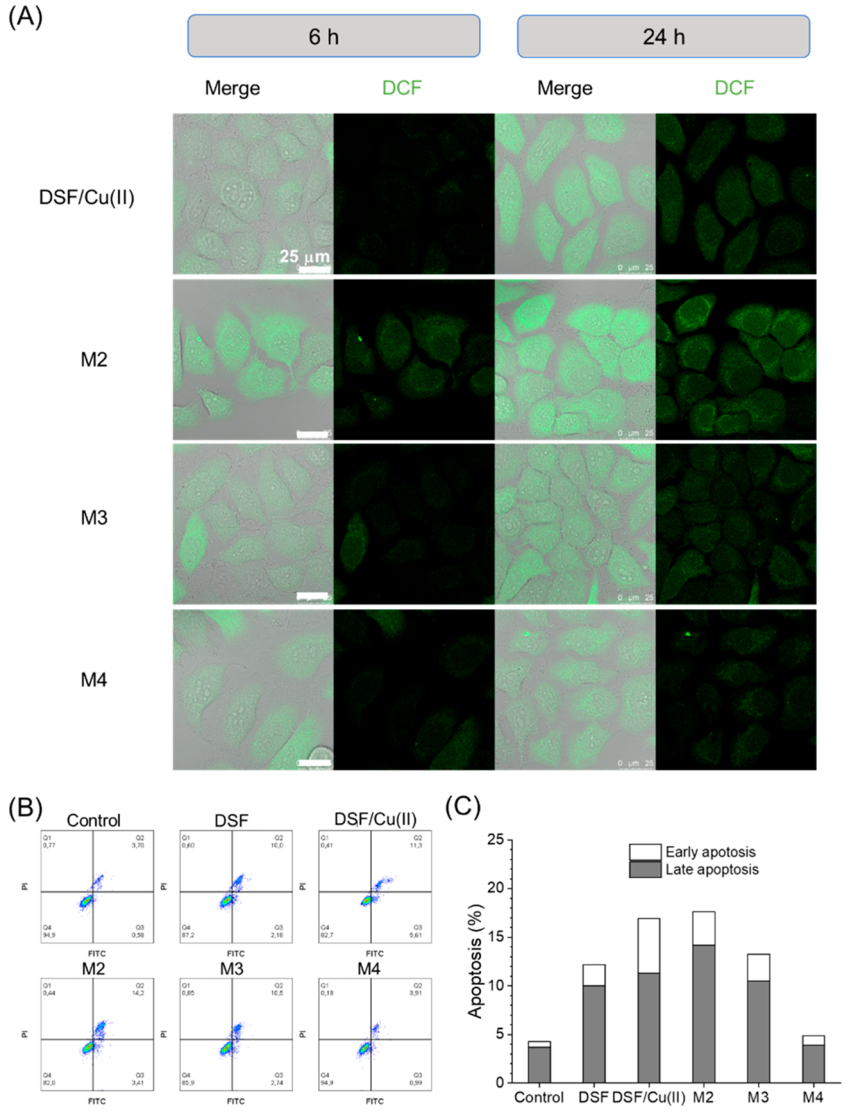


**Figure 7.** (A) CLSM images of A549 cells treated with DSF/Cu(II) and nanoparticles M2−M4 at a DDC concentration of 10 ng/mL for 6 and 24 h. (B, C) Apoptosis rates of A549 cells treated by DSF, DSF/Cu(II), nanoparticles M2−M4 at a DDC concentration of 20 ng/mL for 48 h.

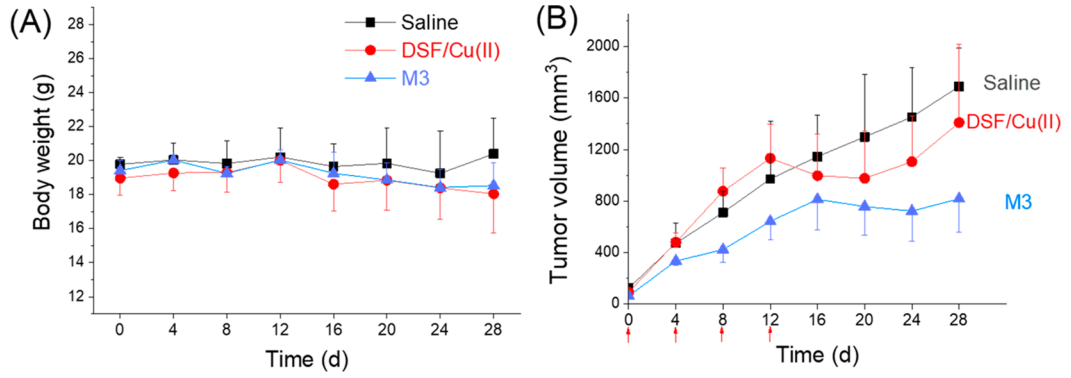


**Figure 8.** Body weights (A) and tumor volumes (B) of tumor-bearing mice treated with saline (control), DSF/Cu(II) (10/1.5 mg/kg), and M3 (1 mg/kg in DSF) on days 0, 4, 8, and 12.

DLC of $Cu(DDC)_2$ showed the least apoptosis. In contrast, M2 and M3 with less DLC of $Cu(DDC)_2$ induced much more apoptosis than M4, which was ascribed to the more internalization of Cu(II) that was in the form of GSH-available Cu(II) rather than in the form of $Cu(DDC)_2$. Cu(II) that coordinated with PEC could react with GSH and $H_2O_2$ successively to give ROS that induced apoptosis.

The more apoptosis induced by M2 and M3 was also confirmed by the cell morphology results. Figure S15 displays the microphotographs of A549 cells that were treated with



DOI: 10.1021/acs.biomac.9b00367
Biomacromolecules XXXX, XXX, XXX−XXX

different formulations (Cu(II) concentrations were 2 μg/mL) for 4 h. Cells treated with M2 and M3 showed obvious shrinkage of cell structures, demonstrating higher apoptosis rates. Overall, we had established that $Cu(DDC)_2$ and the Cu(II) that was not in the form of $Cu(DDC)_2$ in our copper-coordinated nanoparticles enabled chemotherapy and chemodynamic therapy, respectively.

**3.7. *In Vivo* Antitumor Efficacy of Cu(II)/DDC-Loaded Nanoparticles.** The *in vivo* antitumor efficacy of M3 and DSF/Cu(II) was then studied in A549 xenograft nude mice. In the DSF/Cu(II) group, DSF was administrated by intravenous injection at a dose of 10 mg/kg, and Cu(II) was supplemented by oral administration at a dose of 1.5 mg/kg. Given the highly cytotoxic nature of $Cu(DDC)_2$, M3 was intravenously injected with a low dose (1 mg/kg in DSF). The body weights of tumor-bearing mice were monitored, and the results are shown in Figure 8A. There was no significant weight loss in three groups, suggesting the low systemic toxicity of M3. Figure 8B shows the changes of tumor volumes after treatment. DSF/Cu(II) group showed limited antitumor efficacy due to the rapid metabolism of DSF in the blood. In contrast, M3 showed much better antitumor efficacy than saline and DSF/Cu(II) groups considering that the dose of M3 was only equivalent to 10% of the DSF/Cu(II) group. The tumor inhibition rates of DSF/Cu(II) and M3 on day 28 were 16.6% and 51.6%, respectively. The *in vivo* antitumor study demonstrated that our coordination-mediated Cu(II)/DDC-loaded polymeric nanoparticles could efficiently improve the antitumor efficacy of DSF/Cu(II) even at a very low dose. The H&E histological analysis showed that M3 induced more cancer cell necrosis and had negligible toxicity to normal tissues (Figure S16).

## 4. CONCLUSIONS

We reported a coordination strategy for fabrication of Cu(II)- and Cu(II)/DDC-loaded polymeric nanoparticles with excellent stability. Both Cu(II)- and Cu(II)/DDC-loaded polymeric nanoparticles could maintain the nanoparticle properties in neutral and weak acidic pH conditions and upon dilution, which is crucial for its potent *in vivo* biomedical applications such as Cu(II) delivery to address copper-deficiency-related diseases and for cancer therapy. The Cu(II)/DDC-loaded nanoparticles realized combinational cancer therapy of $Cu(DDC)_2$-based chemotherapy and GSH-available Cu(II)-mediated chemodynamic therapy for cancer cells. The *in vivo* study established that Cu(II)/DDC-loaded nanoparticles could remarkedly improve the antitumor efficacy of DSF/Cu(II). The stable metal-coordinated polymeric nanoparticles could provide a new strategy for improving the antitumor efficacy of DSF/Cu(II) and can be expanded to construct a drug delivery platform for combinational chemo/chemodynamic therapy of cancer.

## ■ ASSOCIATED CONTENT

### Supporting Information

The Supporting Information is available free of charge on the ACS Publications website at DOI: 10.1021/acs.biomac.9b00367.

NMR, FTIR, GPC, and other molecular properties of polymers; drug loading contents of Cu(II) and DDC in nanoparticles; other cellular experimental results; H&E results of normal organs and tumors (PDF)

## ■ AUTHOR INFORMATION


### Corresponding Author

*Y. Pu. E-mail: yjpu@scu.edu.cn.

### ORCID

Kui Luo: 0000-0002-3536-1485

Yuji Pu: 0000-0002-4465-0262

Bin He: 0000-0002-0939-9869


### Notes

The authors declare no competing financial interest.

## ■ ACKNOWLEDGMENTS

The authors thank the financial support of National Natural Science Foundation of China (No. 51773130 and 51573111), Fundamental Research Funds for the Central Universities (YJ201764), and Jiangsu international cooperation project (BZ2017062). Dr. Xi Wu in the Analytical & Testing Center, Sichuan University is thanked for his help with ICP-AES testing.

## ■ REFERENCES


(1) Collins, F. S. Mining for therapeutic gold. *Nat. Rev. Drug Discovery* **2011**, *10*, 397.

(2) Iljin, K.; Ketola, K.; Vainio, P.; Halonen, P.; Kohonen, P.; Fey, V.; Grafström, R. C.; Perälä, M.; Kallioniemi, O. High-Throughput Cell-Based Screening of 4910 Known Drugs and Drug-like Small Molecules Identifies Disulfiram as an Inhibitor of Prostate Cancer Cell Growth. *Clin. Cancer Res.* **2009**, *15* (19), 6070−6078.

(3) Chen, D.; Cui, Q. C.; Yang, H.; Dou, Q. P. Disulfiram, a Clinically Used Anti-Alcoholism Drug and Copper-Binding Agent, Induces Apoptotic Cell Death in Breast Cancer Cultures and Xenografts via Inhibition of the Proteasome Activity. *Cancer Res.* **2006**, *66* (21), 10425−10433.

(4) Kim, S. K.; Kim, H.; Lee, D. H.; Kim, T. S.; Kim, T.; Chung, C.; Koh, G. Y.; Kim, H.; Lim, D. S. Reversing the intractable nature of pancreatic cancer by selectively targeting ALDH-high, therapy-resistant cancer cells. *PLoS One* **2013**, *8* (10), e78130.

(5) Liu, P.; Brown, S.; Goktug, T.; Channathodiyil, P.; Kannappan, V.; Hugnot, J. P.; Guichet, P. O.; Bian, X.; Armesilla, A. L.; Darling, J. L.; Wang, W. Cytotoxic effect of disulfiram/copper on human glioblastoma cell lines and ALDH-positive cancer-stem-like cells. *Br. J. Cancer* **2012**, *107* (9), 1488−97.

(6) Li, Y.; Wang, L. H.; Zhang, H. T.; Wang, Y. T.; Liu, S.; Zhou, W. L.; Yuan, X. Z.; Li, T. Y.; Wu, C. F.; Yang, J. Y. Disulfiram combined with copper inhibits metastasis and epithelial-mesenchymal transition in hepatocellular carcinoma through the NF-kappaB and TGF-beta pathways. *J. Cell Mol. Med.* **2018**, *22* (1), 439−451.

(7) Chen, D.; Cui, Q. C.; Yang, H.; Dou, Q. P. Disulfiram, a clinically used anti-alcoholism drug and copper-binding agent, induces apoptotic cell death in breast cancer cultures and xenografts via inhibition of the proteasome activity. *Cancer Res.* **2006**, *66* (21), 10425−33.

(8) Cen, D.; Gonzalez, R. I.; Buckmeier, J. A.; Kahlon, R. S.; Tohidian, N. B.; Meyskens, F. L. Disulfiram Induces Apoptosis in Human Melanoma Cells: A Redox-related Process. *Mol. Cancer Ther.* **2002**, *1* (3), 197−204.

(9) Bakthavatsalam, S.; Sleeper, M. L.; Dharani, A.; George, D. J.; Zhang, T.; Franz, K. J. Leveraging γ-Glutamyl Transferase To Direct Cytotoxicity of Copper Dithiocarbamates against Prostate Cancer Cells. *Angew. Chem., Int. Ed.* **2018**, *57* (39), 12780−12784.

(10) Allensworth, J. L.; Evans, M. K.; Bertucci, F.; Aldrich, A. J.; Festa, R. A.; Finetti, P.; Ueno, N. T.; Safi, R.; McDonnell, D. P.; Thiele, D. J.; Van Laere, S.; Devi, G. R. Disulfiram (DSF) acts as a copper ionophore to induce copper-dependent oxidative stress and mediate anti-tumor efficacy in inflammatory breast cancer. *Mol. Oncol.* **2015**, *9* (6), 1155−68.




DOI: 10.1021/acs.biomac.9b00367
*Biomacromolecules* XXXX, XXX, XXX−XXX

(11) Skrott, Z.; Mistrik, M.; Andersen, K. K.; Friis, S.; Majera, D.; Gursky, J.; Ozdian, T.; Bartkova, J.; Turi, Z.; Moudry, P.; Kraus, M.; Michalova, M.; Vaclavkova, J.; Dzubak, P.; Vrobel, I.; Pouckova, P.; Sedlacek, J.; Miklovicova, A.; Kutt, A.; Li, J.; Mattova, J.; Driessen, C.; Dou, Q. P.; Olsen, J.; Hajduch, M.; Cvek, B.; Deshaies, R. J.; Bartek, J. Alcohol-abuse drug disulfiram targets cancer via p97 segregase adaptor NPL4. *Nature* **2017**, *552* (7684), 194−199.
(12) Song, W.; Tang, Z.; Lei, T.; Wen, X.; Wang, G.; Zhang, D.; Deng, M.; Tang, X.; Chen, X. Stable loading and delivery of disulfiram with mPEG-PLGA/PCL mixed nanoparticles for tumor therapy. *Nanomedicine* **2016**, *12* (2), 377−86.
(13) Wang, Z.; Tan, J.; McConville, C.; Kannappan, V.; Tawari, P. E.; Brown, J.; Ding, J.; Armesilla, A. L.; Irache, J. M.; Mei, Q. B.; Tan, Y.; Liu, Y.; Jiang, W.; Bian, X. W.; Wang, W. Poly lactic-co-glycolic acid controlled delivery of disulfiram to target liver cancer stem-like cells. *Nanomedicine* **2017**, *13* (2), 641−657.
(14) Butcher, K.; Kannappan, V.; Kilari, R. S.; Morris, M. R.; McConville, C.; Armesilla, A. L.; Wang, W. Investigation of the key chemical structures involved in the anticancer activity of disulfiram in A549 non-small cell lung cancer cell line. *BMC Cancer* **2018**, *18* (1), 753−764.
(15) Fasehee, H.; Zarrinrad, G.; Tavangar, S. M.; Ghaffari, S. H.; Faghihi, S. The inhibitory effect of disulfiram encapsulated PLGA NPs on tumor growth: Different administration routes. *Mater. Sci. Eng., C* **2016**, *63*, 587−595.
(16) Zhang, L.; Tian, B.; Li, Y.; Lei, T.; Meng, J.; Yang, L.; Zhang, Y.; Chen, F.; Zhang, H.; Xu, H.; Zhang, Y.; Tang, X. A Copper-Mediated Disulfiram-Loaded pH-Triggered PEG-Shedding TAT Peptide-Modified Lipid Nanocapsules for Use in Tumor Therapy. *ACS Appl. Mater. Interfaces* **2015**, *7* (45), 25147−61.
(17) Duan, X.; Xiao, J.; Yin, Q.; Zhang, Z.; Yu, H.; Mao, S.; Li, Y. Smart pH-sensitive and temporal-controlled polymeric micelles for effective combination therapy of doxorubicin and disulfiram. *ACS Nano* **2013**, *7* (7), 5858−5869.
(18) Wang, C.; Yang, J.; Han, H.; Chen, J.; Wang, Y.; Li, Q.; Wang, Y. Disulfiram-loaded porous PLGA microparticle for inhibiting the proliferation and migration of non-small-cell lung cancer. *Int. J. Nanomed.* **2017**, *12*, 827−837.
(19) Fasehee, H.; Dinarvand, R.; Ghavamzadeh, A.; Esfandyari-Manesh, M.; Moradian, H.; Faghihi, S.; Ghaffari, S. H. Delivery of disulfiram into breast cancer cells using folate-receptor-targeted PLGA-PEG nanoparticles: in vitro and in vivo investigations. *J. Nanobiotechnol.* **2016**, *14*, 32−50.
(20) Huo, Q.; Zhu, J.; Niu, Y.; Shi, H.; Gong, Y.; Li, Y.; Song, H.; Liu, Y. pH-triggered surface charge-switchable polymer micelles for the co-delivery of paclitaxel/disulfiram and overcoming multidrug resistance in cancer. *Int. J. Nanomed.* **2017**, *12*, 8631−8647.
(21) Gupte, A.; Mumper, R. J. Elevated copper and oxidative stress in cancer cells as a target for cancer treatment. *Cancer Treat. Rev.* **2009**, *35* (1), 32−46.
(22) Tao, X.; Gou, J.; Zhang, Q.; Tan, X.; Ren, T.; Yao, Q.; Tian, B.; Kou, L.; Zhang, L.; Tang, X. Synergistic breast tumor cell killing achieved by intracellular co-delivery of doxorubicin and disulfiram via core-shell-corona nanoparticles. *Biomater. Sci.* **2018**, *6* (7), 1869−1881.
(23) Wehbe, M.; Anantha, M.; Shi, M.; Leung, A. W.-Y.; Dragowska, W. H.; Sanche, L.; Bally, M. B. r Development and optimization of an injectable formulation of copper diethyldithiocarbamate, an active anticanceagent. *Int. J. Nanomed.* **2017**, *12*, 4129−4146.
(24) Zhao, P.; Yin, W.; Wu, A.; Tang, Y.; Wang, J.; Pan, Z.; Lin, T.; Zhang, M.; Chen, B.; Duan, Y.; Huang, Y. Dual-Targeting to Cancer Cells and M2Macrophages via Biomimetic Delivery of Mannosylated Albumin Nanoparticles for Drug-Resistant Cancer Therapy. *Adv. Funct. Mater.* **2017**, *27* (44), 1700403.
(25) Chen, W.; Yang, W.; Chen, P.; Huang, Y.; Li, F. Disulfiram Copper Nanoparticles Prepared with a Stabilized Metal Ion Ligand Complex Method for Treating Drug-Resistant Prostate Cancers. *ACS Appl. Mater. Interfaces* **2018**, *10*, 41118−41128.
(26) Zhang, C.; Bu, W.; Ni, D.; Zhang, S.; Li, Q.; Yao, Z.; Zhang, J.; Yao, H.; Wang, Z.; Shi, J. Synthesis of Iron Nanometallic Glasses and Their Application in Cancer Therapy by a Localized Fenton Reaction. *Angew. Chem., Int. Ed.* **2016**, *55* (6), 2101−2106.
(27) Tang, Z.; Liu, Y.; He, M.; Bu, W. Chemodynamic Therapy: Tumour Microenvironment-Mediated Fenton and Fenton-like Reactions. *Angew. Chem., Int. Ed.* **2019**, *58* (4), 946−956.
(28) Tang, Z.; Zhang, H.; Liu, Y.; Ni, D.; Zhang, H.; Zhang, J.; Yao, Z.; He, M.; Shi, J.; Bu, W. Antiferromagnetic Pyrite as the Tumor Microenvironment-Mediated Nanoplatform for Self-Enhanced Tumor Imaging and Therapy. *Adv. Mater.* **2017**, *29* (47), 1701683.
(29) Cheng, F.; Su, T.; Luo, K.; Pu, Y.; He, B. The polymerization kinetics, oxidation-responsiveness, and in vitro anticancer efficacy of poly(ester-thioether)s. *J. Mater. Chem. B* **2019**, *7*, 1005−1016.
(30) Chen, K.; Cai, H.; Zhang, H.; Zhu, H.; Gu, Z.; Gong, Q.; Luo, K. Stimuli-responsive polymer-doxorubicin conjugate: Antitumor mechanism and potential as nano-prodrug. *Acta Biomater.* **2019**, *84*, 339−355.
(31) Pu, Y.; Chang, S.; Yuan, H.; Wang, G.; He, B.; Gu, Z. The anti-tumor efficiency of poly (L-glutamic acid) dendrimers with polyhedral oligomeric silsesquioxane cores. *Biomaterials* **2013**, *34* (14), 3658−3666.
(32) Xu, L.; Yang, Y.; Zhao, M.; Gao, W.; Zhang, H.; Li, S.; He, B.; Pu, Y. A reactive oxygen species-responsive prodrug micelle with efficient cellular uptake and excellent bioavailability. *J. Mater. Chem. B* **2018**, *6* (7), 1076−1084.
(33) Feng, J.; Zhuo, R.-X.; Zhang, X.-Z. Construction of functional aliphatic polycarbonates for biomedical applications. *Prog. Polym. Sci.* **2012**, *37* (2), 211−236.
(34) Li, J.; Zhang, X.; Zhao, M.; Wu, L.; Luo, K.; Pu, Y.; He, B. Tumor-pH-Sensitive PLLA-Based Microsphere with Acid Cleavable Acetal Bonds on the Backbone for Efficient Localized Chemotherapy. *Biomacromolecules* **2018**, *19* (7), 3140−3148.
(35) Liang, Y.; Deng, X.; Zhang, L.; Peng, X.; Gao, W.; Cao, J.; Gu, Z.; He, B. Terminal modification of polymeric micelles with $\pi$-conjugated moieties for efficient anticancer drug delivery. *Biomaterials* **2015**, *71*, 1−10.
(36) Xie, Z.; Guan, H.; Chen, L.; Tian, H.; Chen, X.; Jing, X. Novel biodegradable poly(ethylene glycol)-block-poly(2-methyl-2-carboxyl-propylene carbonate) copolymers: Synthesis, characterization, and micellization. *Polymer* **2005**, *46* (23), 10523−10530.
(37) Xiao, H.; Zhou, D.; Liu, S.; Zheng, Y.; Huang, Y.; Jing, X. A complex of cyclohexane-1,2-diaminoplatinum with an amphiphilic biodegradable polymer with pendant carboxyl groups. *Acta Biomater.* **2012**, *8* (5), 1859−1868.
(38) Roux, A.; Nonat, A. M.; Brandel, J.; Hubscher-Bruder, V.; Charbonnière, L. J. Kinetically Inert Bispidol-Based Cu(II) Chelate for Potential Application to 64/67Cu Nuclear Medicine and Diagnosis. *Inorg. Chem.* **2015**, *54* (9), 4431−4444.
(39) Xin, K.; Li, M.; Lu, D.; Meng, X.; Deng, J.; Kong, D.; Ding, D.; Wang, Z.; Zhao, Y. Bioinspired Coordination Micelles Integrating High Stability, Triggered Cargo Release, and Magnetic Resonance Imaging. *ACS Appl. Mater. Interfaces* **2017**, *9* (1), 80−91.
(40) Gaetke, L. M.; Chow, C. K. Copper toxicity, oxidative stress, and antioxidant nutrients. *Toxicology* **2003**, *189* (1), 147−163.
(41) Ma, B.; Wang, S.; Liu, F.; Zhang, S.; Duan, J.; Li, Z.; Kong, Y.; Sang, Y.; Liu, H.; Bu, W.; Li, L. Self-Assembled Copper-Amino Acid Nanoparticles for In Situ Glutathione "AND" $H_2O_2$ Sequentially Triggered Chemodynamic Therapy. *J. Am. Chem. Soc.* **2019**, *141*, 849−857.
(42) Cen, D.; Brayton, D.; Shahandeh, B.; Meyskens, F. L.; Farmer, P. J. Disulfiram Facilitates Intracellular Cu Uptake and Induces Apoptosis in Human Melanoma Cells. *J. Med. Chem.* **2004**, *47* (27), 6914−6920.
(43) Su, T. A.; Shihadih, D. S.; Cao, W.; Detomasi, T. C.; Heffern, M. C.; Jia, S.; Stahl, A.; Chang, C. J. A Modular Ionophore Platform for Liver-Directed Copper Supplementation in Cells and Animals. *J. Am. Chem. Soc.* **2018**, *140* (42), 13764−13774.


DOI: 10.1021/acs.biomac.9b00367
*Biomacromolecules* XXXX, XXX, XXX−XXX

(44) Liu, Y.; Zhen, W.; Jin, L.; Zhang, S.; Sun, G.; Zhang, T.; Xu, X.; Song, S.; Wang, Y.; Liu, J.; Zhang, H. All-in-One Theranostic Nanoagent with Enhanced Reactive Oxygen Species Generation and Modulating Tumor Microenvironment Ability for Effective Tumor Eradication. *ACS Nano* **2018**, *12* (5), 4886−4893.
(45) Su, T.; Cheng, F.; Yan, J.; Cao, J.; Luo, K.; Pu, Y.; He, B. Hierarchical nanocomposites of graphene oxide and PEGylated protoporphyrin as carriers to load doxorubicin hydrochloride for trimodal synergistic therapy. *J. Mater. Chem. B* **2018**, *6* (28), 4687−4696.
(46) Xu, L.; Zhao, M.; Zhang, H.; Gao, W.; Guo, Z.; Zhang, X.; Zhang, J.; Cao, J.; Pu, Y.; He, B. Cinnamaldehyde-Based Poly(ester-thioacetal) To Generate Reactive Oxygen Species for Fabricating Reactive Oxygen Species-Responsive Nanoparticles. *Biomacromolecules* **2018**, *19* (12), 4658−4667.



DOI: 10.1021/acs.biomac.9b00367
*Biomacromolecules* XXXX, XXX, XXX−XXX